

Bridging the impact response of polymers from the nanoscale to the macroscale

Kyle R. Callahan^{a,b}, Katherine M. Evans^c, William F. Heard^d, Santanu Kundu^{a,b}, Edwin P. Chan^c*

^a Center for Advanced Vehicular Systems, Mississippi State University, Starkville, 39759, MS, United States

^b Dave C. Swalm School of Chemical Engineering, Mississippi State University, Starkville, 39762, MS, United States

^c Materials Science and Engineering Division, National Institute of Standards and Technology, Gaithersburg, 20899, MD, United States

^d Geotechnical and Structure Laboratory, Engineer Research and Development Center, Vicksburg, 39180, MS, United States

ARTICLE INFO

Keywords:

Impact performance

Polymers

Mechanical properties

ABSTRACT

Impact from a fast-moving object is a common event, but it can vary greatly in terms of scale, speed, and energy depending on the specific case. Recently, it has been suggested that scaling analysis can be used to relate the impact performance of materials at the nano- and microscale to their behavior at the macroscale, which is relevant for most applications. In this study, we explore the broad applicability of this approach by conducting micro- and macroprojectile impact tests on polymethyl methacrylate and polycarbonate films. By applying Buckingham Π dimensional analysis to all the impact test results, we demonstrate that the minimum perforation velocity is directly related to the geometric and material properties of each system across a broad range of size and energy scales. Interestingly, we find that the failure stress of the polymer, a critical material property that defines perforation resistance, can be empirically determined based on the deformation of the specific impact test.

1. Introduction

Most people do not need to worry about impact protection on a daily basis. Automobile windshields are designed to protect against road hazards, such as pebbles and rocks that travel at velocities on the order of 20 m s^{-1} [1]. Aircraft and spacecraft can withstand projectiles such as debris or dust particles that impact these vehicles at significantly higher velocities [2,3]. These examples illustrate the variability in impact energies associated with the various impact events because of different projectile sizes and velocities. Fig. 1 illustrates examples of a few impact events demonstrating the broad range of impact energies and size-scale of the deformation.

Traditionally, understanding the impact performance of a material involves studying it with a macroscale projectile impact test, with various projectile materials and sizes traveling up to 2000 m s^{-1} , to identify the critical velocity when perforation occurs [4,5]. However, these tests are expensive, both in terms of the amount of material needed and the time required to conduct them. To address these limitations and facilitate the discovery of new materials, laser-induced projectile impact testing (LIPIT) has been developed as an alternative

means to study the impact performance of ultrathin materials. Here, microprojectiles impact ultrathin films with thicknesses, $h \approx 50 \text{ nm}$ to $1 \mu\text{m}$, and impact velocities ranging from $v_i \approx 100 \text{ m s}^{-1}$ to 1000 m s^{-1} [6]. This combination of high-velocity impacts and ultrathin sample thickness has enabled the characterization of the impact performance of a variety of materials [7–15] at deformation rates from $\approx 10^6 \text{ s}^{-1}$ to 10^8 s^{-1} . Since LIPIT characterizes a material's impact performance at the microscale, the critical question is whether the results translate to the performance of the same material at the macroscale.

Recent studies have addressed this impact performance question by applying various scaling analyses to connect either simulation to LIPIT results [16] or LIPIT to macroscale impact tests [15]. Buckingham Π theory, which involves relating physically similar systems together by arranging key variables into dimensionless quantities [17], has been utilized to connect the impact responses of polycarbonate (PC) from LIPIT to macroscale ballistic experiments [15]. A scaling relationship was developed between the minimum perforation velocity (V_0) and various geometric (film thickness, projectile size) and materials properties (failure stress of polymer, densities). The failure stress (σ_f) of

* Corresponding authors.

E-mail addresses: krc315@msstate.edu (K.R. Callahan), katherine.evans@nist.gov (K.M. Evans), william.f.heard@usace.army.mil (W.F. Heard), santanukundu@che.msstate.edu (S. Kundu), edwin.chan@nist.gov (E.P. Chan).

¹ Contributed equally.

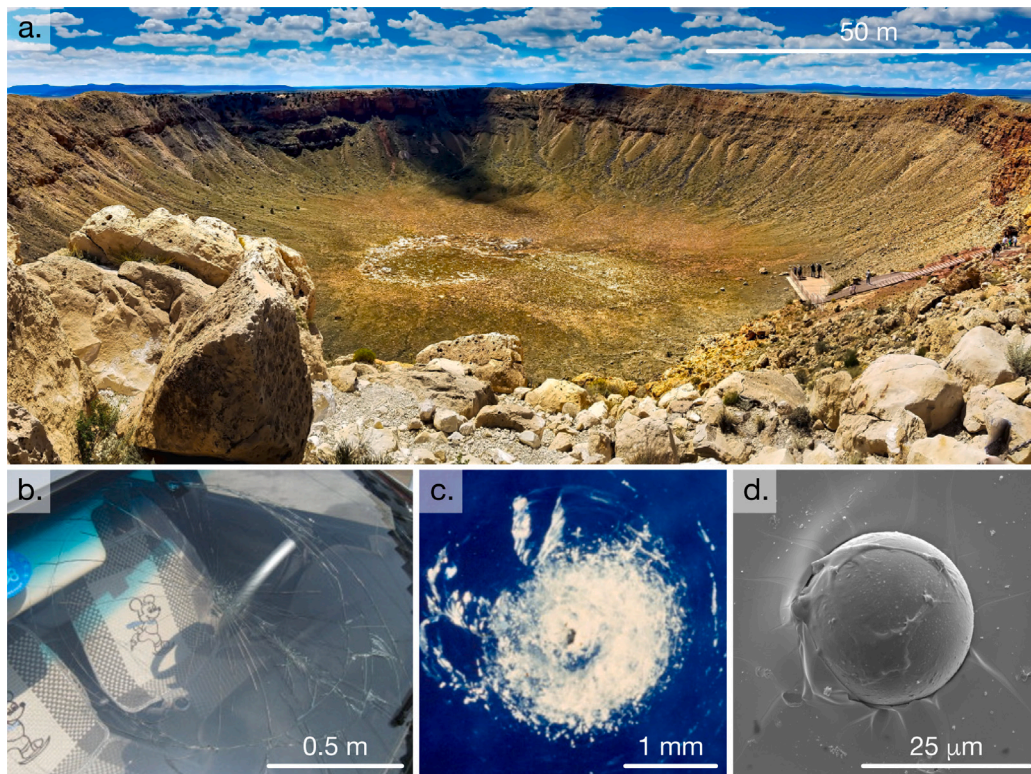


Fig. 1. Examples of impact events in different materials across different energy and size scales. (a) Crater resulting from the collision of a meteorite with Earth [18]. (b) A cracked windshield of a car [1]. (c) Damage resulting from the impact of debris on the space shuttle window [3]. (d) A microparticle embedded into a polycarbonate thin film, captured in a microballistic impact study.

Source: Image adapted from [13].

the polymer, which scaled with both the projectile size and strain rate of the impact test, was shown to be an important material property dictating the impact performance of a material. However, questions remain over the general applicability of this approach and the underlying mechanisms that define it as impact performance is material-specific.

In this work, we address these questions by experimentally studying the impact performance of polymethyl methacrylate (PMMA) and polycarbonate (PC) using both micro- and macroprojectile impact tests. Similar to PC, PMMA is a glassy amorphous polymer. However, PMMA typically exhibits more brittle mechanical behavior than PC during high-velocity impacts [4]. Thus, comparing these two polymers will allow us to gain insight into how a polymer's material properties contribute to its impact performance.

2. Impact testing

2.1. Microprojectile impact studies

Microscale ballistic impact experiments were conducted using LIPIT [13]. A schematic of the test is shown in Fig. 2a. In a typical test, a silica microprojectile of radius $a_p = 10 \mu\text{m}$ (microParticles GmbH) was launched via laser ablation from a launchpad comprised of a $20 \text{ cm} \times 40 \text{ cm}$ glass coverslip substrate, with a 30 nm thick layer of gold, and a $30 \mu\text{m}$, $40 \mu\text{m}$, or $50 \mu\text{m}$ layer of polydimethylsiloxane. The microprojectile then perforated the polymer thin film at an impact velocity v_i and exited the film at a residual velocity v_r . These velocities, measured via an ultrafast camera (Specialized Imaging Ltd, SIMD12) with 20 ns exposure time per frame and an interframe time of 300 ns , are used to calculate the energy dissipation of the film during the impact event based on a kinetic energy balance of an inelastic collision, as discussed below.

PMMA with a number average molecular mass of 267 kg mol^{-1} and polydispersity index of 1.3 was obtained from Polymer Source, Inc.

To prepare PMMA thin films for the LIPIT studies, the polymer was dissolved in toluene, and heated to $\approx 90^\circ \text{C}$ for $\approx 48 \text{ h}$. This solution was filtered using a $0.45 \mu\text{m}$ filter and then spin-coated at 157 rad/sec (1500 rpm) onto a clean silicon wafer substrate. The film thickness, measured using an interferometer (LS-DT2, Filmetrics), was $h \approx 367 \text{ nm}$. The films were then diced into $2 \text{ mm} \times 2 \text{ mm}$ squares with a razor blade and floated off on a water bath. The diced PMMA films were picked up with transmission electron microscopy grids (PELCO, Tabbed 100 mesh, Nickel, Ted Pella, Inc.), dried by wicking with a wipe, and used for the LIPIT measurements without additional processing. Additional details regarding the experimental setup for the LIPIT experiments for PC are located in Chen et al. [13]. We note that the LIPIT results for PC were obtained from a prior study [13].

2.2. Macroprojectile impact studies

Macroscale ballistic impact experiments were conducted using a stationary powder gun with a 1.27 cm internal diameter Mann barrel at the Engineer Research and Development Center (ERDC). Flat sheets ($25.4 \text{ mm} \times 25.4 \text{ mm}$) of PMMA with average thicknesses (h) of 1.4 mm , 2.8 mm , and 5.4 mm were used. PMMA (General Optix by Plaskolite) was purchased from Curbell Plastics. The sample was secured to a frame by clamps before the experiment. To measure the impact (v_i) and residual velocity (v_r) of the projectile, a Phantom TMX 7510 camera was used to film the entire impact event at $180,000$ frames per second. To study the effects of projectile properties on the impact performance, projectiles with two different radii, $a_p = 2.0 \text{ mm}$ and 6.35 mm , were used. The 2.0 mm projectiles were either T4 2017 aluminum (Al) with a density $\rho_p = 2790 \text{ kg m}^{-3}$ or S2 Rockbit steel (St) with a density $\rho_p = 7790 \text{ kg m}^{-3}$. The 6.35 mm projectiles were exclusively S2 Rockbit steel. Four-piece nylon sabots fit the various projectiles to the internal diameter of the rifle barrel. A separator plate, placed downstream from the gun, intercepted the sabot pieces

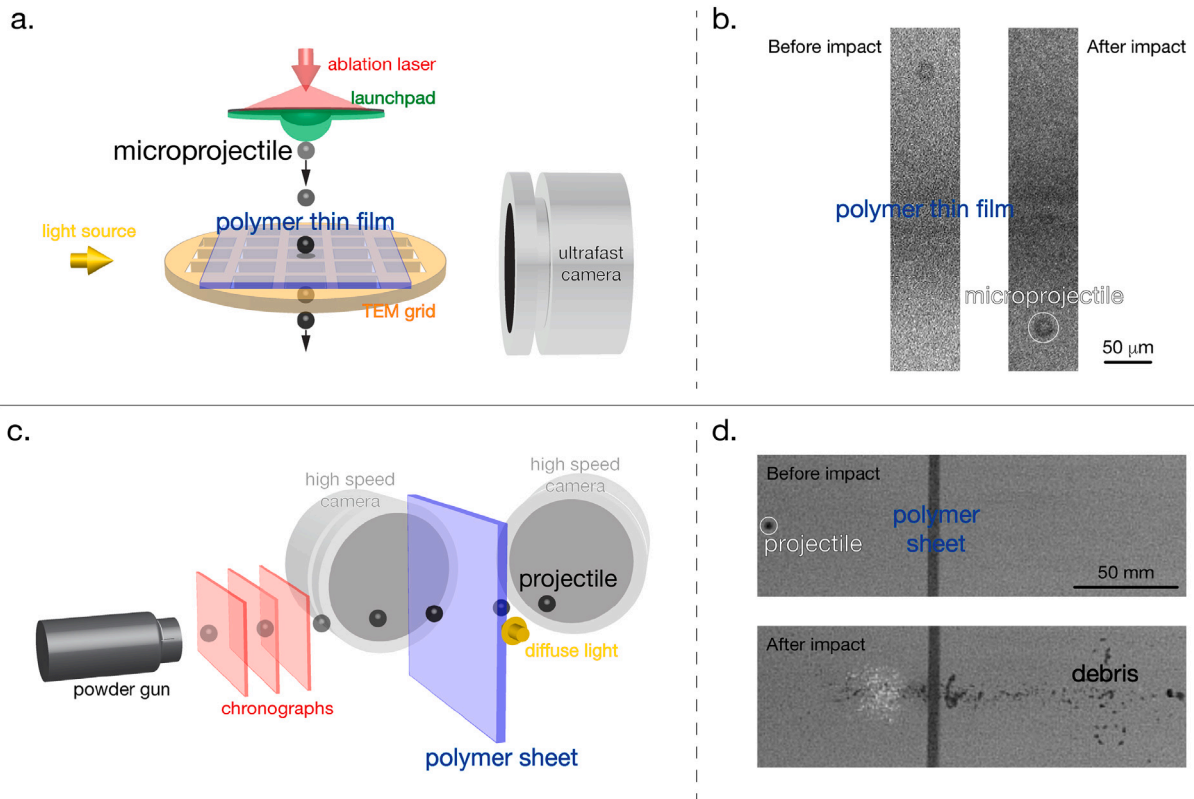


Fig. 2. Microscale and macroscale ballistic impact experiments used in this study. (a) Schematic depicting LIPIT instrument used for the microscale ballistic impact experiments. (b) Representative images of a LIPIT experiment showing the microprojectile before and after impacting the polymer thin film. The side-view images show the microprojectile moving from top to bottom. (c) Schematic depicting the powder gun setup used for the macroscale ballistic experiments. (d) Representative images recorded before and after the projectile impacting a 6.35 mm thick PMMA sheet. The side-view images show the projectile moving from left to right.

while allowing clear passage to the projectile. Measured quantities of N165 powder propellant controlled the impact velocity of the projectile package. A set of four chronographs measured the impact velocity and the effects of drag on the projectile. All macroscopic experiments using PC may be found in Callahan et al. [19]

3. Results

The results of the impact tests for both PMMA and PC are shown in Fig. 3. Fig. 3a is a plot of v_r^2 vs. v_i^2 for PMMA from both the micro- and macroprojectile impact tests for all the different geometric and material configurations. We find that $v_r < v_i$ for all the tests, which indicates that energy is dissipated by the polymer during the impact event.

To determine the extent of energy dissipation and compare across the different energy scales, we fit the results using the normalized kinetic loss expression that characterizes the perforation event as an inelastic collision between the projectile and the polymer film [13,15],

$$v_r^2 = \alpha v_i^2 - \gamma \quad (1)$$

where the parameters α and γ are extracted from Fig. 3a and correspond to the slope and Y -intercept, respectively. The parameter $\alpha = m_p/(m_p + m)$ characterizes the projectile's mass (m_p) relative to the system's mass participating in the impact ($m_p + m$). Here, m is defined as the mass of the polymer film participating in the impact. The parameter $\gamma = E_d/(m_p + m)$ is the energy dissipation (E_d) of the polymer film normalized by the system's mass.

The α and γ values from each test are summarized in Table 1. By substituting these values into Eq. (1), we calculate the expected residual impact energy ($\alpha v_i^2 - \gamma$) as a function of impact velocity. By comparing the experimentally measured v_r^2 with $\alpha v_i^2 - \gamma$ (Fig.

3b), we find that all data sets collapse onto a master curve without any adjustable parameters. Both micro- and macro-scale experiments follow Eq. (1) without the need for additional fitting parameters to account for scale differences. This is striking as the comparison is made across all the different impact test configurations where the impact energies span from nanojoules to kilojoules, as observed for micro- and macroprojectiles impact, respectively.

From these results, we can determine the minimum perforation velocity (V_0), which defines the critical impact velocity when the polymer film completely arrests a projectile ($v_r = 0$). This parameter has been used as a parameter to quantify the impact performance of many different impact mitigating materials and is defined as [15],

$$V_0 = \left(\frac{\gamma}{\alpha}\right)^{1/2} \quad (2)$$

The V_0 values for PMMA as a function of the size ratio of polymer to the projectile (h/a_p) are shown in Fig. 3c.

Fig. 3d summarizes v_r^2 vs. v_i^2 for PC from both the micro- and macroprojectile impact tests. We use the previously reported α , γ , and V_0 parameters, and the values are also summarized in Table 1. Similar to PMMA, the plot of v_r^2 with $\alpha v_i^2 - \gamma$ (Fig. 3e) also shows that all PC data sets collapse onto a master curve without any adjustable parameters. We again use the minimum perforation velocity to evaluate the performance of PC films, and the results are shown in Fig. 3f.

4. Discussion

As shown in Fig. 3b and e, rescaling the impact energies for both the PMMA and PC systems demonstrates that we can compare the results for different impact testing methods, material types, and test geometries. The results in Fig. 3c and f show a positive correlation between the size ratio and impact performance for both polymer systems.

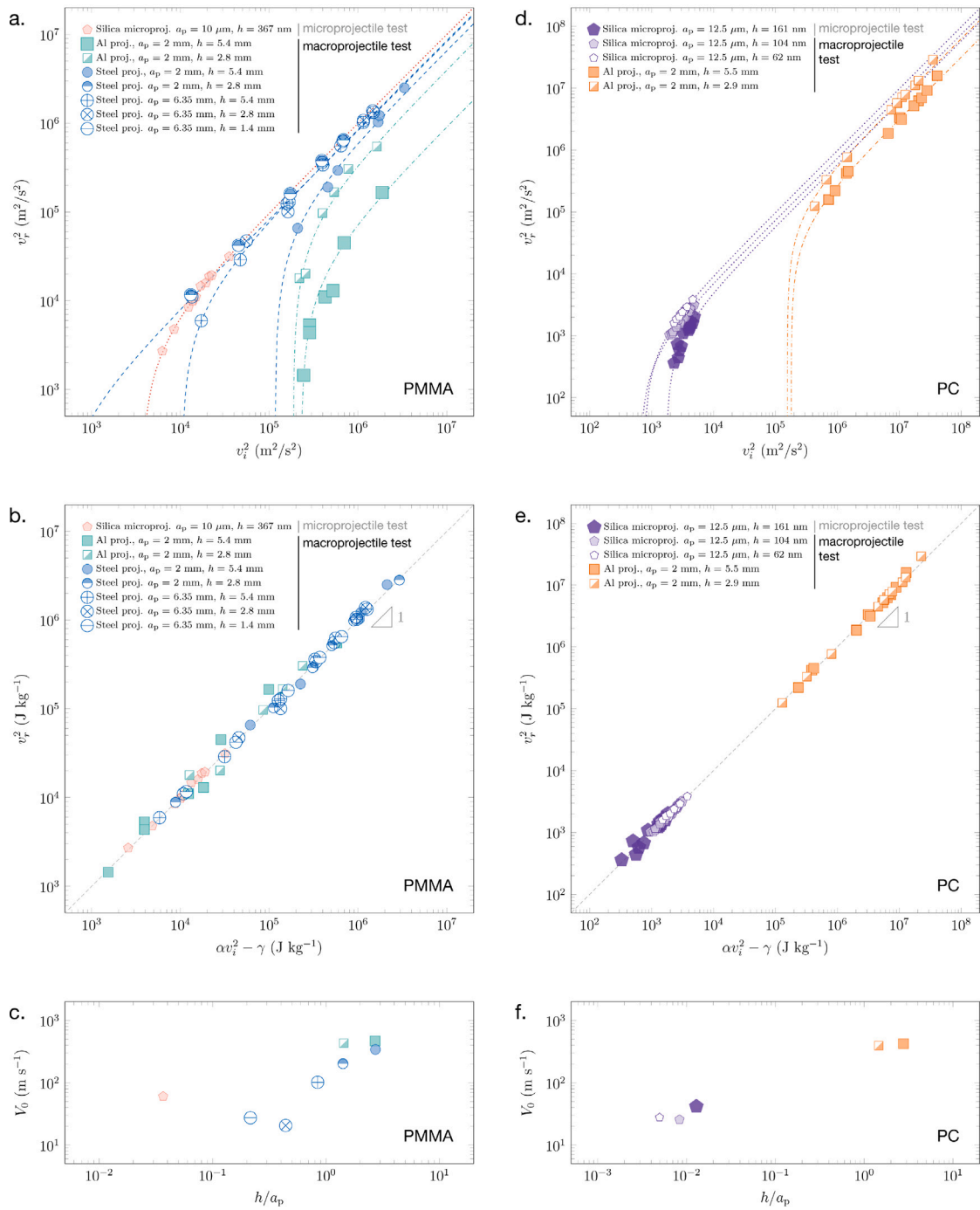


Fig. 3. Macroprojectile and microprojectile impact test results for polymethyl methacrylate (PMMA) and polycarbonate (PC). (a) Residual velocity squared (v_r^2) versus impact velocity squared (v_i^2) results for PMMA. The curves are fits to the data used to extract the α and γ parameters. (b) Rescaling the impact results for PMMA using Eq. (1), which is the normalized kinetic energy loss expression that compares the impact across different energy scales. (c) Minimum perforation velocity V_0 versus film thickness to projectile radius ratio (h/a_p) for PMMA. (d) v_r^2 versus v_i^2 results for PC. The curves are fits to the data used to extract the α and γ parameters. (e) Rescaling the impact results for PC using Eq. (1). (f) V_0 versus h/a_p for PC.

For PMMA, the minimum perforation velocity generally increases with increasing polymer film thickness or decreasing projectile size as the highest $V_0 \approx 470 \text{ m s}^{-1}$ for $h/a_p = 2.71$ was obtained from macroscale ballistic testing with an aluminum projectile. Surprisingly, the lowest minimum perforation velocity is not associated with the smallest size ratio, i.e., the microballistic impact testing using silica microprojectiles, thus suggesting that size nor mass ratio alone does not define impact performance. It is important to note this trend could be because the PMMA used for the different scale tests are obtained from different sources. Unlike the PMMA systems, the results for PC (Fig. 3f) show

a strong correlation between the geometry of the test configuration and performance; V_0 increases with h/a_p , which suggests that impact performance improves with increasing PC film thickness or decreasing projectile size.

To understand how the various materials and geometric properties couple to define impact performance, we applied Buckingham Π dimensional analysis on the impact results for PMMA and PC. We use the Buckingham Π dimensional relationships defined by Evans et al. [15] to show that the minimum perforation velocity is a function of the

Table 1
Summary of materials parameters obtained from macroscale and microscale ballistic impact experiments.

Material	Thickness, h (mm)	Density, ρ (kg m ⁻³)	Proj. material (mm)	Proj. radius, a_p (mm)	Proj. density (kg m ⁻³)	α	γ (m ² s ⁻²)	V_0 (m s ⁻¹)
PMMA	5.4 ± 0.11	1180	Aluminum	2	2790	0.059	13,052	467
PMMA	2.8 ± 0.11	1180	Aluminum	2	2790	0.40	75,382	432
PMMA	5.4 ± 0.05	1180	Steel	2	7790	0.66	77,363	342
PMMA	2.8 ± 0.14	1180	Steel	2	7790	0.77	31,624	203
PMMA	5.4 ± 0.13	1180	Steel	6.35	7790	0.86	8868	102
PMMA ^a	2.8 ± 0.16	1180	Steel	6.35	7790	0.83	351	21
PMMA ^a	1.4 ± 0.05	1180	Steel	6.35	7790	0.95	714	27
PMMA ^c	3.67 × 10 ⁻⁴	1180	Silica	1 × 10 ⁻²	2650	1	3661	61
PC	5.5 ± 0.03	1200	Aluminum	2	2790	0.32	57,199	425
PC	2.9 ± 0.05	1200	Aluminum	2	2790	0.63	97,561	394
PC ^{b,c}	1.61 × 10 ⁻⁴	1180	Silica	2.5 × 10 ⁻²	2650	0.58	1006	42
PC ^{b,c}	1.04 × 10 ⁻⁴	1180	Silica	2.5 × 10 ⁻²	2650	0.74	487	26
PC ^{b,c}	6.2 × 10 ⁻⁵	1180	Silica	2.5 × 10 ⁻²	2650	0.98	753	28

^a Not used for the Buckingham Π dimensional analysis.

^b Parameters obtained from [15].

^c Denote LIPIT experiments, the remaining ones are powder-gun experiments.

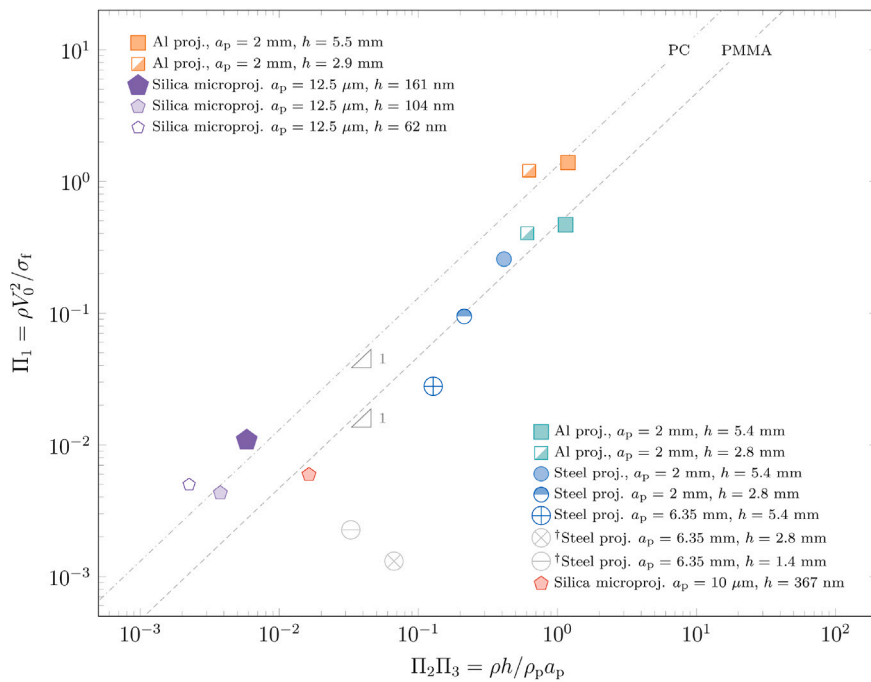


Fig. 4. Buckingham Π dimensional analysis of the micro and macro-scale ballistic impact data for PMMA and PC. Note that the data points marked with \dagger were omitted from the scaling analysis.

geometric properties (a_p, h) and materials properties (ρ_p, ρ, σ_f),

$$\begin{aligned} \Pi_1 &= \frac{\rho V_0^2}{\sigma_f} \\ \Pi_2 &= \frac{h}{a_p} \\ \Pi_3 &= \frac{\rho}{\rho_p} \end{aligned} \quad (3)$$

with,

$$\Pi_1 = c_0 \Pi_2 \Pi_3 \quad (4)$$

where c_0 is a proportionality constant. As estimated from Fig. 4, the values for PMMA and PC are c_0 0.47 and 1.31, respectively. These values suggest that c_0 is not a universal constant and thus specific to the polymer. While the complex nature of a ballistic impact will depend on additional inelastic properties such as dissipation zone size, fracture toughness, etc, which are material-specific properties incorporated into c_0 , our application of the Buckingham Π analysis aims to simplify such

details by identifying the primary parameter most crucial for impact performance.

The parameter Π_2 considers the importance of the volume of the polymer material ($\approx \pi a_p^2 h$) relative to that of the projectile ($\approx \pi a_p^3$). The parameter Π_3 considers the importance of the density of the polymer material (ρ) versus that of the projectile (ρ_p).

The parameter Π_1 defines the ratio of the impact energy of the projectile at the minimum perforation velocity ($\approx V_0^2$) versus the specific impact resistance of the polymer ($\approx \sigma_f / \rho$). It was previously suggested that the yield stress of the polymer (σ_Y) is a good estimate of σ_f at these deformation rates [15]. This assumption is particularly suitable for brittle polymeric materials. We make a similar approximation of σ_f for our materials.

The prior approach extrapolated σ_Y by developing a correlation plot between Π_1 and $\Pi_2 \Pi_3$. Here, we applied mechanical models from Kolsky bar testing of PMMA and PC, connected to the specific polymer dynamics, to experimentally determine σ_Y and incorporate these values into our Buckingham Π analysis. For PMMA, Acharya et al. related the

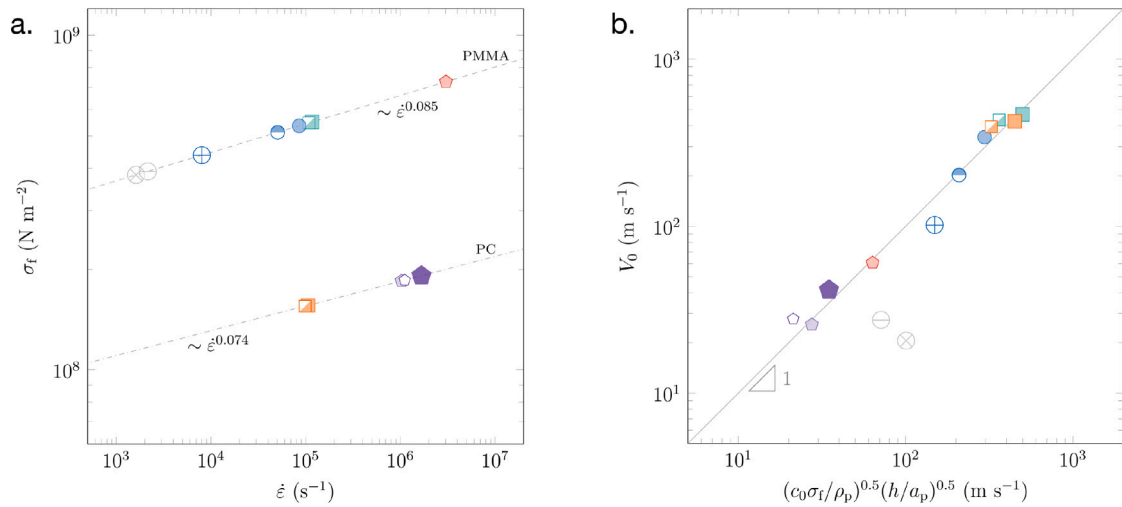


Fig. 5. Relationship between materials properties and impact performance. (a) Determination of the failure stress of PMMA and PC using Eqs. (5) and (6), respectively. These fits are shown in dotted lines (b) Relating the minimum perforation velocity of PMMA and PC with the geometric and materials properties of the materials systems.

yield stress to the deformation rate ($\dot{\epsilon}$) as [20],

$$\sigma_Y \cong 204\dot{\epsilon}^{0.085} \quad (5)$$

For PC, Mulliken and Boyce established that the yield stress is related to the deformation rate as [21,22],

$$\sigma_Y \cong 66\dot{\epsilon}^{0.074} \quad (6)$$

Using these relationships, we determine the failure stress of PMMA and PC as a function of deformation rate. The deformation rate is approximated as $\dot{\epsilon} \approx V_0/2a_p$ [8,13,15]. The results are summarized in Fig. 5a, and suggest that the failure stress of PMMA is greater than PC across all the strain rates, which is consistent with prior studies that showed PC to exhibit significantly higher toughness than PMMA [23,24]. As can be seen in from the fits in Figs. 4 and 5b, using Eqs. (5) and (6) to calculate σ_Y was successful.

It is perhaps surprising that the relationship between yield stress and strain rate holds at the strain rates studied here, up to three orders of magnitude greater than was previously established. However, this can be explained by understanding the underlying mechanisms that dictate the mechanical behavior of these polymers. Using an Eyring-type yield model, Mulliken and Boyce proposed a rate- and temperature-dependent mechanical model that connected the macroscopic mechanical behavior to molecular origins that can be decomposed into the contributions of different molecular motions, each with their own unique rate and temperature dependence for both polymers [21].

At low strain rates or high temperatures, the α -relaxation, *i.e.* glass transition temperature (T_g), is the dominant process for energy dissipation in polymers. With increasing strain rate or decreasing temperature, the contribution from β relaxation and other sub- T_g relaxations becomes more prominent. For PC, the β -relaxation is primarily associated with the molecular motions of the phenyl groups along the polymer backbone [21]. Other molecular motions, such as rotations of methyl groups and cis-trans conformational changes of the carbonate groups, have also been suggested to contribute to the sub- T_g relaxations of PC [25,26]. Prior research has suggested that these molecular relaxations facilitate ductility in PC even below its T_g [23].

PMMA also exhibits β -relaxation, and it has been shown that it is associated with the flipping of the ester group along the polymer backbone and methyl group rotations [27]. However, it is convoluted with the α -relaxation at high frequencies [21]. Dielectric thermal analysis (DETA) results, provided in the supplementary information, also show that the β -relaxation peak merges with the α -relaxation peak at frequencies $>10^4 \text{ s}^{-1}$. At higher testing frequencies, we expect that the molecular motions associated with the β -relaxation are coupled with

the α -relaxation. As such, the sub- T_g relaxations do not appear in the DETA results for the frequencies and temperatures examined here. The unique combination of α - and β -relaxation in PC and PMMA determines their mechanical response in the experiments shown here. Although more work is needed, the DETA results would suggest that β -relaxations remain active for PC even at the higher test frequencies, which is consistent with the notion that PC is a tougher material compared with PMMA [23,24]. Additionally, we remark that V_0 is a metric for quantifying the amount of impact energy the material can withstand. It does not describe the mode of failure or how the material dissipates the impact energy.

From the discussions above, it is clear that the yield stress, a surrogate for σ_f , of the material defines impact performance in a ballistic impact experiment. However, this property alone does not define overall impact performance and we can show this by rearranging Eq. (4). In doing so, we establish a relationship between the minimum perforation velocity, a metric for evaluating impact performance, and the various materials and geometric properties that contribute to impact performance,

$$V_0 = \left(c_0 \frac{\sigma_f}{\rho_p} \right)^{1/2} \left(\frac{h}{a_p} \right)^{1/2} \quad (7)$$

The results of this relationship are shown in Fig. 5b. Importantly, these results illustrate the various strategies for achieving similar impact performance levels depending on the constraints of a particular application. Using the PC results as an example, we see that the V_0 increases with increasing h/a_p , thus demonstrating that geometry is one approach to control impact performance. Alternatively, the failure stress of the material is another strategy to control impact performance. This is demonstrated when we compare the powder-gun results between PMMA and PC impacted by an aluminum projectile. Since their h/a_p ratios are similar, the differences in impact performance can be attributed to the relative differences in σ_f . As such, the V_0 for PMMA is slightly greater than PC at similar values of h/a_p since the failure stress for PMMA is greater than PC.

5. Conclusion

In this work, we conducted experimental micro- and macroscale ballistic impact tests on polymethyl methacrylate and polycarbonate films using spherical projectiles of different sizes and films of different thicknesses. We demonstrated that the minimum perforation velocity, a metric used to assess impact performance, is related to the system's

geometric and materials properties. Buckingham *II* dimensional analysis was successfully applied to compare all the impact test results to understand the effects of energy scale, size scale, and materials properties on impact performance. We show that this scaling analysis can provide insight into different polymeric materials. Furthermore, it validates small-scale tests for screening a particular material for its impact mitigation properties.

Besides demonstrating that this methodology enables comparison of impact performance independent of the impact energy, from nanojoules to kilojoules, our results reveal that the strain-rate dependent yield stress of the polymer, which can be measured using other impact tests at much lower strain rates ($<10^4 \text{ s}^{-1}$), is a parameter that defines the perforation resistance for these materials at these ultrahigh strain rates.

CRedit authorship contribution statement

Kyle R. Callahan: Writing – review & editing, Writing – original draft, Formal analysis, Data curation. **Katherine M. Evans:** Writing – review & editing, Writing – original draft, Formal analysis, Data curation, Conceptualization. **William F. Heard:** Data curation. **Santanu Kundu:** Writing – review & editing, Supervision, Formal analysis, Conceptualization. **Edwin P. Chan:** Writing – review & editing, Writing – original draft, Supervision, Conceptualization.

Declaration of competing interest

The authors declare that they have no known competing financial interests or personal relationships that could have appeared to influence the work reported in this paper.

Acknowledgments

Certain instruments and materials were identified in this paper to adequately specify the experimental details. Such identification does not imply recommendation by the National Institute of Standards and Technology, nor does it imply that the materials are necessarily the best available for the purpose.

This research was partially conducted at Mississippi State University, United States under contract to the U.S. Department of Defense (DoD) Military Engineering, through the US Army Engineer Research and Develop Center (ERDC) Contract #W912HZ21C0022. The views and conclusions contained herein are those of the authors and should not be interpreted as necessarily representing the official policies or endorsements, either expressed or implied, of the U.S. Army ERDC or the U.S. DoD.

DISTRIBUTION A. Approved for public release; distribution unlimited.

Appendix A. Supplementary data

Supplementary material related to this article can be found online at <https://doi.org/10.1016/j.eml.2025.102331>.

Data availability

Data will be made available on request.

References

- [1] J. Xu, Y. Li, X. Chen, Y. Yan, D. Ge, M. Zhu, B. Liu, Characteristics of windshield cracking upon low-speed impact: Numerical simulation based on the extended finite element method, *Comput. Mater. Sci.* 48 (3) (2010) 582–588, <http://dx.doi.org/10.1016/j.commatsci.2010.02.026>, URL <https://linkinghub.elsevier.com/retrieve/pii/S0927025610000947>.
- [2] W. Schonberg, F. Schäfer, R. Putzar, Hypervelocity impact response of honeycomb sandwich panels, *Acta Astronaut.* 66 (3–4) (2010) 455–466, <http://dx.doi.org/10.1016/j.actaastro.2009.06.018>, URL <https://linkinghub.elsevier.com/retrieve/pii/S0094576509003531>.
- [3] G. Drolshagen, Impact effects from small size meteoroids and space debris, *Adv. Space Res.* 41 (7) (2008) 1123–1131, <http://dx.doi.org/10.1016/j.asr.2007.09.007>, URL <https://linkinghub.elsevier.com/retrieve/pii/S0273117707009416>.
- [4] A.J. Hsieh, D. DeSchepper, P. Moy, P.G. Dehmer, J.W. Song, The Effects of PMMA on Ballistic Impact Performance of Hybrid Hard/Ductile All-Plastic- and Glass-Plastic-Based Composites, *Tech. Rep. A878024*, 2004.
- [5] M.E. Backman, W. Goldsmith, The mechanics of penetration of projectiles into targets, *Internat. J. Engrg. Sci.* 16 (1) (1978) 1–99, [http://dx.doi.org/10.1016/0020-7225\(78\)90002-2](http://dx.doi.org/10.1016/0020-7225(78)90002-2), URL <https://www.sciencedirect.com/science/article/pii/0020722578900022>.
- [6] D. Veysset, J.-H. Lee, M. Hassani, S.E. Kooi, E.L. Thomas, K.A. Nelson, High-velocity micro-projectile impact testing, *Appl. Phys. Rev.* 8 (1) (2021) 011319, <http://dx.doi.org/10.1063/5.0040772>, URL <https://aip.scitation.org/doi/10.1063/5.0040772>.
- [7] J.-H. Lee, D. Veysset, J.P. Singer, M. Retsch, G. Saini, T. Pezeril, K.A. Nelson, E.L. Thomas, High strain rate deformation of layered nanocomposites, *Nat. Commun.* 3 (2012) 1164, <http://dx.doi.org/10.1038/ncomms2166>, URL <http://www.nature.com/ncomms/journal/v3/n10/full/ncomms2166.html>.
- [8] J.-H. Lee, P.E. Loya, J. Lou, E.L. Thomas, Dynamic mechanical behavior of multilayer graphene via supersonic projectile penetration, *Science* 346 (6213) (2014) 1092–1096, <http://dx.doi.org/10.1126/science.1258544>, URL <http://science.sciencemag.org/content/346/6213/1092>.
- [9] R. Thevamaran, O. Lawal, S. Yazdi, S.-J. Jeon, J.-H. Lee, E.L. Thomas, Dynamic creation and evolution of gradient nanostructure in single-crystal metallic microcubes, *Science* 354 (6310) (2016) 312–316, <http://dx.doi.org/10.1126/science.aag1768>, URL <http://science.sciencemag.org/content/354/6310/312>.
- [10] S. Xue, Z. Fan, O.B. Lawal, R. Thevamaran, Q. Li, Y. Liu, K.Y. Yu, J. Wang, E.L. Thomas, H. Wang, X. Zhang, High-velocity projectile impact induced 9R phase in ultrafine-grained aluminium, *Nat. Commun.* 8 (1) (2017) 1653, <http://dx.doi.org/10.1038/s41467-017-01729-4>, URL <https://www.nature.com/articles/s41467-017-01729-4>.
- [11] J. Hyon, O. Lawal, O. Fried, R. Thevamaran, S. Yazdi, M. Zhou, D. Veysset, S.E. Kooi, Y. Jiao, M.-S. Hsiao, J. Streit, R.A. Vaia, E.L. Thomas, Extreme energy absorption in glassy polymer thin films by supersonic micro-projectile impact, *Mater. Today* 21 (8) (2018) 817–824, <http://dx.doi.org/10.1016/j.mattod.2018.07.014>, URL <http://www.sciencedirect.com/science/article/pii/S1369702117309677>.
- [12] E.P. Chan, W. Xie, S.V. Orski, J.-H. Lee, C.L. Soles, Entanglement density-dependent energy absorption of polycarbonate films via supersonic fracture, *ACS Macro Lett.* 8 (2019) 806–811.
- [13] S.H. Chen, A.J. Souna, C.L. Soles, S.J. Stranick, E.P. Chan, Using microprojectiles to study the ballistic limit of polymer thin films, *Soft Matter* 16 (2020) 3886–3890, <http://dx.doi.org/10.1039/D0SM00295J>, URL <https://pubs.rsc.org/en/content/articlelanding/2020/sm/d0sm00295j>.
- [14] J. Hyon, M. Gonzales, J.K. Streit, O. Fried, O. Lawal, Y. Jiao, L.F. Drummy, E.L. Thomas, R.A. Vaia, Projectile impact shock-induced deformation of one-component polymer nanocomposite thin films, *ACS Nano* 15 (2) (2021) 2439–2446, <http://dx.doi.org/10.1021/acsnano.0c06146>.
- [15] K.M. Evans, S.H. Chen, A.J. Souna, S.J. Stranick, C.L. Soles, E.P. Chan, The projectile perforation resistance of materials: Scaling the impact resistance of thin films to macroscale materials, *ACS Appl. Mater. Interfaces* 15 (27) (2023) 32916–32925, <http://dx.doi.org/10.1021/acscami.3c05130>, URL <https://doi.org/10.1021/acscami.3c05130>, Publisher: American Chemical Society.
- [16] Y. Cheng, J. Dong, F. Li, Y. Shen, Q. An, K. Xiao, M. Jiang, Y. Liu, C. Huang, X. Wu, W.A. Goddard, Scaling law for impact resistance of amorphous alloys connecting atomistic molecular dynamics with macroscale experiments, *ACS Appl. Mater. Interfaces* 15 (10) (2023) 13449–13459, <http://dx.doi.org/10.1021/acscami.2c19719>, URL <https://pubs.acs.org/doi/10.1021/acscami.2c19719>.
- [17] E. Buckingham, On physically similar systems; illustrations of the use of dimensional equations, *Phys. Rev.* 4 (4) (1914) 345–376, <http://dx.doi.org/10.1103/PhysRev.4.345>, URL <https://link.aps.org/doi/10.1103/PhysRev.4.345>.
- [18] C. Natale, Winslow’s meteor crater impresses the world, *EastVally. Com* (2020) URL https://www.eastvalleytribune.com/get_out/winslow-s-meteor-crater-impresses-the-world/article_a220505e-ba2e-11ea-a89a-276ed4662cac.html.
- [19] K. Callahan, W.F. Heard, S. Kundu, High strain rate failure behavior of polycarbonate plates due to hypervelocity impact, *Macromolecules* 55 (21) (2022) 9640–9649.
- [20] S. Acharya, A.K. Mukhopadhyay, High strain rate compressive behavior of PMMA, *Polym. Bull.* 71 (1) (2014) 133–149, <http://dx.doi.org/10.1007/s00289-013-1050-9>, URL <http://link.springer.com/10.1007/s00289-013-1050-9>.

- [21] A.D. Mulliken, M.C. Boyce, Mechanics of the rate-dependent elastic–plastic deformation of glassy polymers from low to high strain rates, *Int. J. Solids Struct.* 43 (5) (2006) 1331–1356, <http://dx.doi.org/10.1016/j.ijsolstr.2005.04.016>, URL <http://www.sciencedirect.com/science/article/pii/S0020768305002313>.
- [22] S. Sarva, M. Boyce, Mechanics of polycarbonate during high-rate tension, *J. Mech. Mater. Struct.* 2 (10) (2007) 1853–1880, <http://dx.doi.org/10.2140/jomms.2007.2.1853>, URL <https://msp.org/jomms/2007/2-10/p01.xhtml>.
- [23] C.L. Soles, A.B. Burns, K. Ito, E. Chan, J. Liu, A.F. Yee, M.S. Tyagi, Importance of sub-nanosecond fluctuations on the toughness of polycarbonate glasses, *Macromolecules* 53 (15) (2020) 6672–6681, <http://dx.doi.org/10.1021/acs.macromol.0c00857>, URL <https://pubs.acs.org/doi/10.1021/acs.macromol.0c00857>.
- [24] C.L. Soles, A.B. Burns, K. Ito, E.P. Chan, J.F. Douglas, J. Wu, A.F. Yee, Y.-T. Shih, L. Huang, R.M. Dimeo, M. Tyagi, Why enhanced subnanosecond relaxations are important for toughness in polymer glasses, *Macromolecules* 54 (5) (2021) 2518–2528, <http://dx.doi.org/10.1021/acs.macromol.0c02574>, URL <https://pubs.acs.org/doi/10.1021/acs.macromol.0c02574>.
- [25] J.Y. Jho, A.F. Yee, Secondary relaxation motion in bisphenol a polycarbonate, *Macromolecules* 24 (8) (1991) 1905–1913, <http://dx.doi.org/10.1021/ma00008a031>, URL <https://pubs.acs.org/doi/abs/10.1021/ma00008a031>.
- [26] C. Xiao, J.Y. Jho, A.F. Yee, Correlation between the shear yielding behavior and secondary relaxations of bisphenol a polycarbonate and related copolymers, *Macromolecules* 27 (10) (1994) 2761–2768, <http://dx.doi.org/10.1021/ma00088a017>, URL <https://pubs.acs.org/doi/abs/10.1021/ma00088a017>.
- [27] K. Schmidt-Rohr, A.S. Kulik, H.W. Beckham, A. Ohlemacher, U. Pawelzik, C. Boeffel, H.W. Spiess, Molecular nature of the .beta. relaxation in poly(methyl methacrylate) investigated by multidimensional NMR, *Macromolecules* 27 (17) (1994) 4733–4745, <http://dx.doi.org/10.1021/ma00095a014>, URL <https://pubs.acs.org/doi/abs/10.1021/ma00095a014>.